

Img2CAD: Reverse Engineering 3D CAD Models from Images through VLM-Assisted Conditional Factorization

Yang You
Stanford University
Stanford, CA, USA
yangyou@stanford.edu

Mikaela Angelina Uy
Stanford University
Stanford, CA, USA
mikacuy@cs.stanford.edu

Jiaqi Han
Stanford University
Stanford, CA, USA
jiaqihan@stanford.edu

Rahul Thomas
Stanford University
Stanford, CA, USA
rt03mas@stanford.edu

Haotong Zhang
Peking University
Beijing, China
2200012835@stu.pku.edu.cn

Suya You
The U.S. Army Research Lab
Maryland, USA
suya.you.civ@army.mil

Leonidas Guibas
Stanford University
Stanford, CA, USA
guibas@cs.stanford.edu

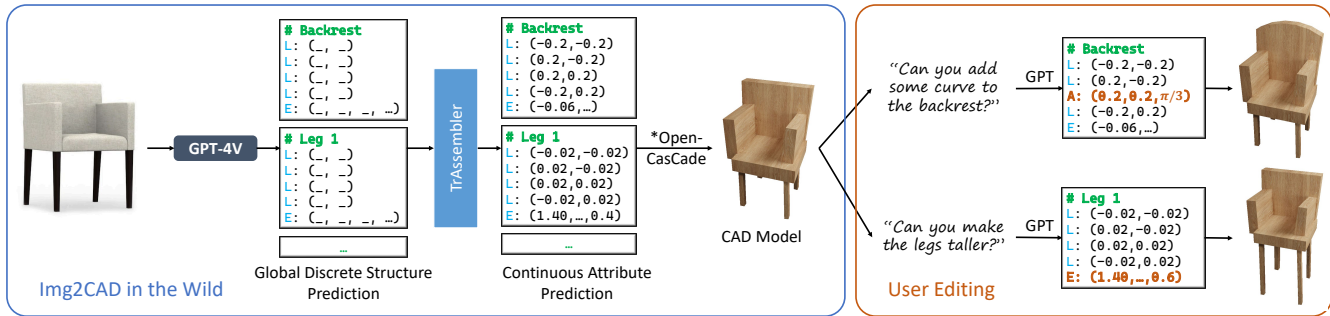


Figure 1: Img2CAD: A Framework for Reverse Engineering 3D CAD Models from Single-View Images. Our method leverages GPT-4V to predict the discrete CAD program structure and then uses a semantic-conditioned transformer to predict the continuous attributes. This approach allows users to easily reconstruct and edit a CAD model from a single-view input image. We use OpenCasCade [Cag Gemini [n. d.]] to convert the CAD program back to a 3D mesh.

Reverse engineering 3D computer-aided design (CAD) models from images is an important task for many downstream applications including interactive editing, manufacturing, architecture, robotics, etc. The difficulty of the task lies in vast representational disparities between the CAD output and the image input. CAD models are precise, programmatic constructs that involves sequential operations combining discrete command structure with continuous attributes – making it challenging to learn and optimize in an end-to-end fashion. Concurrently, input images introduce inherent challenges such as photo-metric variability and sensor noise, complicating the reverse engineering process. In this work, we introduce a novel approach that conditionally factorizes the task into two sub-problems. First, we leverage large foundation models, particularly GPT-4V, to

predict the global *discrete base structure* with semantic information. Second, we propose TrAssembler that conditioned on the discrete structure with semantics predicts the *continuous attribute* values. To support the training of our TrAssembler, we further constructed an annotated CAD dataset of common objects from ShapeNet. Putting all together, our approach and data demonstrate significant first steps towards CAD-ifying images in the wild. Our project page: anonymous123342.github.io

1 INTRODUCTION

A vast array of human-made objects in our everyday environments are created using computer-aided design (CAD) [Várady et al. 1997]. Reverse engineering the structural CAD representation [Buonamici et al. 2018] from raw sensor input is an essential task that enables the fabrication of 3D shapes and their manipulation or editing for various downstream applications, such as manufacturing, design, and robotics. The beauty of a CAD representation lies in its elegant structure, which combines *discrete* operation types with *continuous* attribute parameters. This results in a programmatic, parameterized

Authors’ addresses: Yang You, Stanford University, Stanford, CA, 94305, USA, yangyou@stanford.edu; Mikaela Angelina Uy, Stanford University, Stanford, CA, 94305, USA, mikacuy@cs.stanford.edu; Jiaqi Han, Stanford University, Stanford, CA, 94305, USA, jiaqihan@stanford.edu; Rahul Thomas, Stanford University, Stanford, CA, 94305, USA, rt03mas@stanford.edu; Haotong Zhang, Peking University, Beijing, China, 2200012835@stu.pku.edu.cn; Suyu You, The U.S. Army Research Lab, Maryland, USA, suya.you.civ@army.mil; Leonidas Guibas, Stanford University, Stanford, CA, 94305, USA, guibas@cs.stanford.edu.

structure that allows for easy and intuitive editing and manipulation.

Previous works [Li et al. 2023; Ren et al. 2022; Uy et al. 2022] have explored reverse engineering 3D CAD models from input point clouds, which require 3D sensor inputs. However, images are much more common for everyday objects, such as those captured with smartphones or found in product images via Google search. This makes the task of reverse engineering CAD models from images particularly important and useful. The image-to-CAD problem presents significant challenges, as we typically only obtain a single view of the object in the form of pixels, while the CAD representation demands a detailed understanding of the object’s whole 3D geometry.

Reverse engineering CAD models from input images poses two significant challenges: *generalization* and *representation complexity*. The first challenge lies in the ability of the models to generalize across diverse images, particularly when these images originate from heterogeneous sources. Images from different sources will give different viewing angles, lighting conditions, sensor noise and textures, which makes training a generalizable model from image directly to CAD extremely difficult. This problem is even more severe as there is a lack of CAD data available for common objects in everyday life (e.g., chairs and tables).

Secondly, CAD systems, despite their utility in applications requiring detailed editing and manipulation, present significant challenges due to its combination of discrete command types with continuous parameter values. A CAD model is a sequence of discrete geometric operations of different types, e.g. line, arc, circle, extrude add, extrude cut – each characterized by continuous attributes such as length, position, and angle. Learning this dual nature of both *discrete* operations and their *continuous* attributes poses a non-trivial challenge, necessitating algorithms to predict both the structural and attribute components accurately. The hybrid *discrete-continuous* nature of the problem makes image-to-CAD learning and optimization non-trivial. This approach may require an exponential amount of data to learn a combinatorial space of structures, which is difficult to obtain.

To tackle these problems, we propose to conditionally factorize the task into two sub-problems – to first predict the global *discrete base structure* and then, *conditioned* on this base structure, to regress the *continuous attribute values*. For the first part, we leverage the generalizability of large vision foundation models, particularly GPT-4V, to predict the global base structure from an image. We then propose a transformer-based network named **TrAssembler**, to regress the continuous attributes conditioned on the discrete structure. While the space of possible object structures is vast, even within a single category such as chairs, shared substructures among objects are extremely common. For example, many chairs have support structures consisting of four legs. Moreover, we find that a VLM can generate semantically consistent part labels as program comments for such common substructures. These labels can then be used by the continuous attribution prediction network to effectively establish correspondences that facilitate communication and shared learning across *corresponding attributes* (e.g., leg length) of different objects, thus enabling the sharing of information across the attribute space. Our conceptual idea is inspired by the mathematical

notion of sheaves [Curry 2014], where fibers (the attribute parameter spaces in our case) over points in a base space (the space of labelled CAD structures in our case) have partial locally consistent structure (through *corresponding attributes*).

To train TrAssembler, we further introduce a CAD dataset of common objects. This was constructed by leveraging the rich part annotations of PartNet [Mo et al. 2019b] and the general assistance of VLMs – resulting in our CAD-ified subset of ShapeNet [Chang et al. 2015]. Our experiments demonstrate the feasibility of our approach for image-to-CAD, which, to the best of our knowledge, is the first of its kind for a general sketch-extrude CAD representation of common objects. We show that our method outperforms baselines and further showcase various applications, such as CAD-ification and shape editing from images in the wild.

2 RELATED WORKS

2.1 Reverse Engineering CAD

Reverse engineering in CAD has been a well-studied focus in computer graphics and CAD communities [Benkő et al. 2002; Benko and Varady 2004; Bénére et al. 2013; Ma et al. 2023; Várady et al. 1997], allowing for the structured representation of shapes for different tasks such as editing and manufacturing. Initial works explored reconstructing CAD through inverse CSG modeling [Du et al. 2018; Kania et al. 2020; Ren et al. 2021; Sharma et al. 2018; Yu et al. 2023] that decomposes shapes into simple volumes combined with boolean operations. Despite being effective for reconstruction, these methods often involve numerous components with a decomposition that is not compact, making them less flexible and harder to be manipulated by users. Recent advancements have been driven by large-scale CAD datasets (ABC [Koch et al. 2019], Fusion 360 [Willis et al. 2021], SketchGraphs [Seff et al. 2020]) that enabled the development of data-driven techniques for B-Rep classification [Jayaraman et al. 2021], segmentation [Dupont et al. 2022; Jayaraman et al. 2021; Lambourne et al. 2021], parametric surface inference [Guo et al. 2022; Liu et al. 2023], CAD reconstruction [Khan et al. 2024; Lambourne et al. 2022] and generation [Xu et al. 2023]. Different from these datasets that mostly consist of mechanical parts, one of our contributions is a CAD dataset of common every day objects that contain meaningful semantic parts, allowing for more natural user editing.

In reverse engineering, a prevalent CAD modeling approach employs the *sketch-extrude* [Uy et al. 2022; Willis et al. 2021] paradigm, where a sketch [Para et al. 2021; Xu et al. 2022] is defined as a series of parametric curves forming a closed loop, resulting in flexible and complex primitives, which is the focus of this work. Some recent works have borrowed ideas from NLP to interpret CAD models as sequences of tokens [Ganin et al. 2021; Jayaraman et al. 2023; Wu et al. 2021; Zhang et al. 2024]. Point2Cyl [Uy et al. 2022] takes a different approach and redefines the CAD reverse engineering task as a geometry-aware decomposition problem. It decomposes an input point cloud into extrusion cylinders (sketch-extrude primitives), and subsequent works extended this approach to the unsupervised [Ren et al. 2022] and self-supervised [Li et al. 2023] settings. These works however take in 3D point clouds as input; in contrast, our work tackles a more challenging setting with a single-view image input.

2.2 Structured Representation of Shapes

Our daily objects are often highly structured in their geometry and part composition. For example, a chair is composed of parts governed by a set of rules and constraints [Ritchie et al. 2023; Uy et al. 2020, 2021], such as having legs of equal lengths placed symmetrically around the seat. Existing works have explored various ways of representing and learning structure from shapes, such as part-based templates [Ganapathi-Subramanian et al. 2018; Kim et al. 2013; Ovsjanikov et al. 2011], symmetries [Mitra et al. 2006; Sung et al. 2015], shape programs [Jones et al. 2020, 2021, 2023; Müller et al. 2023], and grammars [Chaudhuri et al. 2011; Kalogerakis et al. 2012]. Notably, GRASS [Li et al. 2017] and StructureNet [Mo et al. 2019a] represent a shape as a graph of part hierarchies learned through a supervised neural network. The goal of this line of work is to learn higher-level semantic structures, i.e., parts of shapes, but does not focus the reconstruction of the local geometric detail of each part. These methods typically assume a coarse and homogeneous representation for each part, commonly as bounding boxes. In contrast, our goal is to address image-to-CAD for daily objects, which requires not only understanding the underlying structure but also reconstructing each part’s geometry.

2.3 Primitive Fitting

Another relevant area in computer graphics is primitive fitting. One line of work involves decomposing shapes into surface or volumetric primitives. Classical graphics approaches include detecting simple primitives such as planes [Czerniawski et al. 2018; Fang et al. 2018; Monzpart et al. 2015] using methods like RANSAC [Li et al. 2011; Schnabel et al. 2007], region growing [Oesau et al. 2016], or Hough voting [Borrmann et al. 2011; Drost and Ilic 2015]. Data-driven approaches [Lê et al. 2021; Li et al. 2019; Sharma et al. 2020] have also grown in popularity, leveraging models that fit simple primitives such as planes, cylinders, cones, and spheres.

Primitive fitting has also been used for shape abstraction, approximating shapes with cuboids [Tulsiani et al. 2017; Zou et al. 2017] or superquadrics [Paschalidou et al. 2019, 2020] given an input shape. This line of work more commonly take 3D point clouds as input in primitive recovery. Moreover, these works also assume a fixed predefined set of primitives, whereas our work represent shapes as CAD program and thus recovers more general primitives defined by arbitrary closed loop, hence explaining more general objects.

Similar to our CAD representation, learning the primitive decomposition or shape abstractions of a shape allows for intuitive shape editing [Li et al. 2019] and manipulation [Sung et al. 2020]. Notably, ReparamCAD [Kodnongbua et al. 2023] is a relevant recent work that learns the variation space given only a single model, though it assumes an underlying shape program (also in the form of boxes) given as input. In contrast, our work learns to output the underlying CAD program given only a single input image without assuming a predefined set of primitives.

3 BACKGROUND: SKETCH-EXTRUDE CAD

Before diving into the specifics of our method, we first provide some background and define the general *sketch-extrude* primitives that we use to represent shapes in this work. We adopt a popular industrial standard for reverse engineering shapes into a sequence of sketch

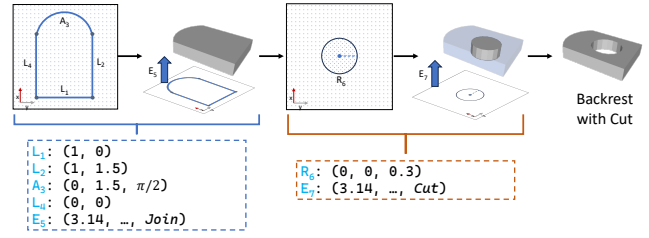


Figure 2: An illustrative example of a sketch and extrusion command sequence for a chair’s backrest with a circular cutout. The backrest is created using two extrusion blocks: the first one employs the sketch commands *lines* and *arcs* with the extrusion type *NewBody*, while the second one uses the sketch command *circles* with the extrusion type *Cut*.

and extrude commands, as used in solid modeling softwares such as OpenCascade [Cappgemini [n. d.]], Fusion360 [Autodesk 2021], and Solidworks [Systèmes 2005]. These tools enable the creation of a wide array of shapes, as they do not assume a finite set of primitives but can represent any geometry that is a composition of primitives created by the *extrusion* of any non-self-intersecting, closed *sketch* loop. Below, we define the different types of discrete commands in this CAD language and their corresponding continuous attributes.

Sketch. A sketch is defined as any closed, non-self-intersecting loop drawn on a 2D plane, where each loop is called a profile. A profile is created with a sequence of sketch commands of three different types – *lines* (L), *arcs* (A), and *circles* (R). The continuous attributes for each type of sketch command are as follows:

- $L : (x, y)$, where (x, y) defines the endpoint of a line segment¹.
- $A : (x, y, \alpha)$ where (x, y) is the endpoint of an arc with a sweep angle α .
- $R : (x, y, r)$, which defines a circle with the center (x, y) and radius r .

To result in a valid sketch profile, the resulting curve from the series of commands must be closed and non-self-intersecting².

Extrusion. In manufacturing, extrusion is the process of pushing sketches forward along a fixed cross-sectional profile to a desired distance, creating a volumetric solid, often referred to as an extrusion cylinder [Uy et al. 2022]. Extrusion cylinders are then combined through either join or cut operations to form the final model. We distinguish between an extrusion *join* and an extrusion *cut* as two distinct command types in this work.

The continuous attributes of the extrusion command are given as $E : (\alpha, \theta, \gamma, x, y, z, e)$, where (α, θ, γ) are the three Euler angles defining the extrusion coordinate frame, (x, y, z) denote the origin of the extrusion coordinate system, and e represents the extrusion distance or extent³.

Figure 2 shows an illustrative example of the sketch-extrude CAD language, comprising discrete command types and their continuous

¹Modellers typically assume that the starting point of the first line segment is at the origin.

²Without loss of generality, we require sketches to be constructed in a counter-clockwise direction.

³Note that in our implementation, there is an additional b argument specifying whether it is a join or cut. As defined, we regard this as two different command types.

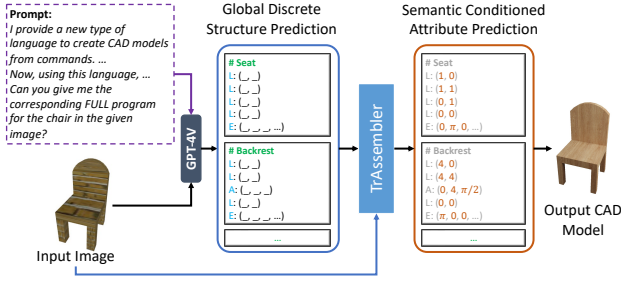


Figure 3: Overview of our two-stage pipeline. The first stage involves GPT-4V interpreting the input image to decompose it into semantic parts and generate a sequence of discrete CAD structures. The second stage uses a transformer-based model to predict continuous attributes for each part.

attribute values. The discrete command types define the structure of the underlying shape – in this case the backrest – while the attributes continuously vary the shape’s geometry. For example, changing the third argument in the R command will enlarge the cut.

4 METHOD

Reverse engineering a 3D model from input images is a challenging task in computer graphics and vision due to the discrete-continuous nature of the problem. This task requires learning the combinatorial space of shape and program structure along with their corresponding continuous attributes.

Our approach addresses the challenging image-to-CAD problem for common objects by *conditionally factorizing* the task into two sub-problems. First, we leverage the capabilities of large foundation models (i.e., GPT-4V [Achiam et al. 2023]) to predict the *global discrete base structure* of the shape from a single input image. This discrete problem involves inferring the *semantic parts* present in the image and providing the *CAD structure*, i.e., the command types of each underlying part. Subsequently, we propose a novel transformer-based network called **TrAssembler** that, conditioned on this semantic discrete base structure, predicts the *continuous attributes* for the sequence of CAD commands for each semantic part. An overview of the pipeline is shown in Figure 3 and we elaborate on each component in the following subsections.

4.1 Discrete Global Structure with GPT-4V

In this work, we define the *global discrete base structure* of a shape as both its part decomposition and the CAD command types for each underlying part. Inferring a shape’s discrete base structure from a single image is challenging due to the combinatorial nature of the problem and the difficulty of generalization across diverse input images from heterogeneous sources. Learning such a model would typically require vast, possibly exponential, amounts of data. Therefore, we leverage large foundation models, specifically GPT-4V [Achiam et al. 2023], which has been trained on extensive amounts of textual and visual data of common objects, such as furniture, to tackle this challenge.

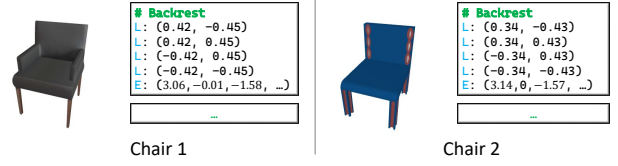


Figure 4: Different chairs still share similar part semantics, and similar parts share similar attribute parameters, facilitating easier attribute prediction.

Concretely, we prompt the VLM to infer the discrete global structure by explaining the CAD sketch-extrude language, utilizing in-context learning [Alayrac et al. 2022] by providing a simple example and an additional common object example. Most critically, we employ the chain-of-thought [Wei et al. 2022] technique by asking it to first list the semantic parts from the given image before predicting the CAD sequence for each part.

Furthermore, we prompt the VLM to provide *semantic part comments* in its predicted global base structure. This involves attaching a part label, i.e., a program comment, before providing the CAD sequence for each identified part. We observe that VLMs’ knowledge of object structure and their ability to perceive it in an image enables consistent labeling regardless of the underlying global structure.

This semantic labeling is crucial as it facilitates communication and shared learning across corresponding attributes of different objects in our attribute prediction network. This design allows for sharing between shapes with common substructures, even when they have different global discrete base structures.

For example, as shown in Figure 4, backrests from different chairs, recognized and parsed by GPT-4V, are represented within distinct semantic structural blocks, yet the ground-truth CAD commands for these blocks share similar parameters such as axis of extrusion, dimensions, and extrusion distances.

4.2 TrAssembler – Continuous Attribute Prediction in Shared Space

Our exploration led to the finding that, despite GPT-4V showing promise in inferring the discrete base structure – part semantics and their underlying sequence of command types – it exhibits limitations in accurately predicting the continuous attributes of CAD commands. Figure 6 illustrates a failure case of GPT-4V. To address this shortcoming, we introduce TrAssembler, which takes in a single image and, conditioned on the discrete base structure from GPT-4V, predicts the *continuous attributes* for all CAD commands.

Specifically, TrAssembler is a transformer-based architecture that conditions on the base structure from GPT-4V, represented as a sequence of commands $[C_k^j]$ for $k \in 1, 2, \dots, N_j$ and a semantic part comment y_j for each part P_j for all parts, i.e., $j \in 1, 2, \dots, M$, where M is the number of parts in GPT-4V’s predicted structure and N_j is the number of CAD commands for part P_j . TrAssembler then predicts the continuous attribute values for each command C_k^j for all parts P_j . Since the underlying continuous attribute values differ for each CAD command type (line, arc, circle, extrude), similar to [Wu et al. 2021], we unify them into a common output space that can be predicted by a shared network structure.

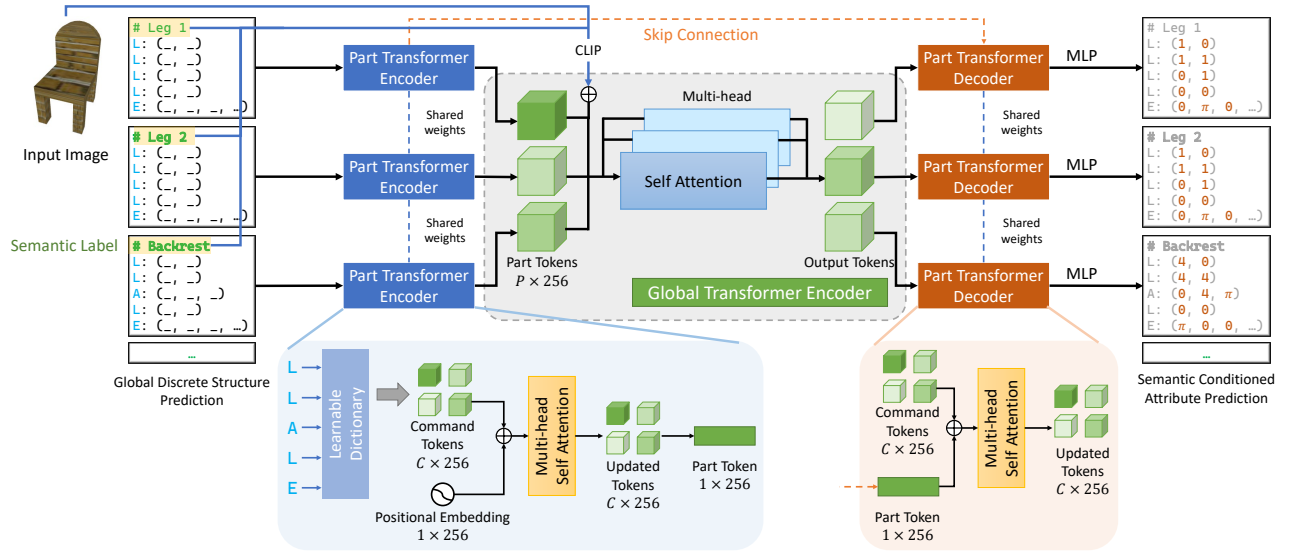


Figure 5: Overall architecture of TrAssembler. The model first leverages part transformer encoder to generate part embeddings with part structures given by GPT-4V. The part embeddings are then fed into a global transformer encoder and refines them with multi-head self-attention, followed by an MLP to decode the final attribute parameters for each command.

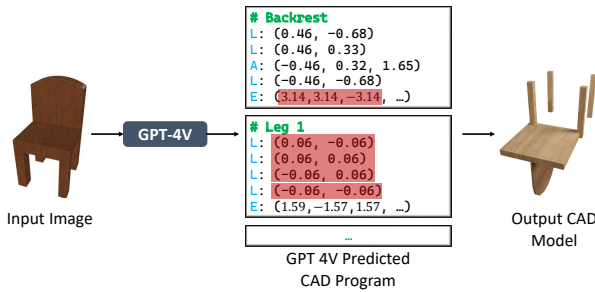


Figure 6: Illustration of GPT-4V’s limitations in predicting continuous attributes. While GPT-4V effectively decomposes and labels parts, it struggles with accurate prediction of continuous attributes such as the leg’s scale and backrest’s extension direction (marked in red).

Architecture Details. Figure 5 shows the network architecture of TrAssembler. Each part P_j , including the CAD structure or command types along with the part comments, is first fed into a part transformer encoder. This encoder transforms each command type into latent embeddings using a learnable dictionary and performs multi-head self-attention on the sequence of commands to obtain a corresponding sequence of command tokens $\{W_k^j \mid W_k^j \in \mathbb{R}^{256}\}$. These command tokens are aggregated into a single part token $T_j \in \mathbb{R}^{256}$ via summation, which serves as the learned vector for each discrete part from GPT-4V. Since assembling a shape requires understanding the correlation and interaction between different parts, TrAssembler employs a global transformer encoder that conducts global attention across all parts. Specifically, each learned part token T_j is concatenated with an image latent embedding and part comment y_j embedding for global structure information through the image, and for semantic information through the part comment, respectively. Both the image and the semantic part comment are

encoded with CLIP [Radford et al. 2021]. The global transformer encoder outputs a list of refined part tokens $\{\hat{T}_j \mid \hat{T}_j \in \mathbb{R}^{256}\}$ that are semantically-informed and global structure-aware. Finally, our part transformer decoder concatenates the refined part token \hat{T}_j to each command token W_k^j for the sequence of commands for each part P_j . It then performs multi-head self-attention across all commands in P_j , which is subsequently fed into an MLP to predict the continuous attribute values for each command.

A core innovation of TrAssembler lies in its utilization of the discrete structure provided by GPT-4V. By conditioning on this discrete structure, the continuous attribute prediction becomes significantly easier, as the image-to-CAD task conditioned on the discrete base structure simplifies into a continuous problem. Also critical to our TrAssembler is its hierarchical transformer design, comprising the part and global transformers, and its use of consistent semantic labels from GPT-4V. These elements facilitate information sharing across the attribute space, which our experiments show is essential for achieving better performance. Additionally, our design choice of using transformer-based architectures enables the handling of varying numbers of parts M of shapes and different numbers of commands N_j for parts. This flexibility is crucial for accommodating the diverse and complex nature of CAD tasks.

5 DATASET

We need to train TrAssembler with the ground-truth attribute parameters for each part. Therefore, a substantial, curated CAD dataset is necessary. Previous resources such as the ABC dataset [Koch et al. 2019] offer extensive CAD data; however, these datasets predominantly focus on industrial components and are less applicable to domestic items like chairs and tables. To address this gap and

Table 1: Image to CAD reconstruction results comparison on CAD-ified Chair, Table, and Cabinet test dataset.

	Chair			Table			Cabinet		
	CD ↓	Seg Acc (%) ↑	Seg mIoU (%) ↑	CD ↓	Seg Acc (%) ↑	Seg mIoU (%) ↑	CD ↓	Seg Acc (%) ↑	Seg mIoU (%) ↑
GPT-Only	0.3806	50.49	34.96	0.3676	62.16	41.99	0.3807	54.66	47.65
Image-3D-CAD	0.3549	49.26	34.86	0.4232	48.52	35.57	0.4558	57.76	54.98
DeepCAD	0.2914	70.44	54.86	0.3633	60.20	46.50	0.3310	62.70	54.95
DeepCAD-End2End	0.2346	77.01	65.06	0.3698	67.37	52.21	0.3279	60.55	53.23
Ours	0.1685	81.79	73.32	0.1655	83.75	69.55	0.2327	66.32	57.33



Figure 7: Data samples from our curated CAD dataset. For each pair, left: ShapeNet model, right: our CAD-ified model.

further facilitate CAD research on everyday objects, we have compiled a CAD-ified dataset of common objects encompassing three classes from ShapeNet [Chang et al. 2015]: *chair*, *table*, and *cabinet*.

For dataset creation, we employ a hybrid method that capitalizes on GPT-4V’s structural priors in a semi-automatic fashion. Initially, we input segmented per-part images (since we have the ground-truth segmentation) into GPT-4V, which then predicts the semantic label and the corresponding lines, arcs, and circles for each part. Subsequently, utilizing the ground-truth labels, we perform one-to-one part label matching using the linear sum assignment method [Burkard et al. 2012]. For each matched part prediction, we adjust the ground-truth 3D mesh to correct the scale and translation errors introduced by GPT-4V’s assembly inaccuracies. Adjustments are made to sketch endpoints and extrusion distances in order to align with the ground-truth scale, while the extrusion plane’s origin is repositioned for accurate translation. Additionally, arcs and circles require special treatment for scaling, as direct scaling could deform a circle into an oval, which is not feasible in standard CAD commands. To overcome this, we employ the RANSAC method [Fischler and Bolles 1981] to accurately fit the parameters for arcs and circles. This hybrid approach has proven to yield superior data quality.

Post data generation, each example undergoes manual review to ensure high fidelity, culminating in a comprehensive dataset comprising 1,026 chairs, 3,243 tables, and 305 cabinets. We follow PartNet [Mo et al. 2019b] train/val/test splits. To the best of our knowledge, this is the first large-scale dataset for common domestic objects, and it is intended to serve as a benchmark for training and evaluating CAD-related tasks on common objects.

6 EXPERIMENTS

In this section, we evaluate our proposed method named **Img2CAD** for reverse engineering 3D CAD models from images of various common objects. Additionally, we conduct ablation studies to verify the efficacy of our key design elements in the pipeline. Lastly, we show that our method is robust to images from arbitrary viewpoints.

Baselines. We consider the following four baselines:

- *GPT-Only*: This baseline directly employs the output CAD program from GPT-4V without our attribute prediction network.
- *Image-3D-CAD*: Since most CAD-related works require a 3D mesh as input, we build this baseline to test how well current CAD reconstruction methods perform when converting a 2D image to 3D. We first use Point-E [Nichol et al. 2022] to predict the corresponding point cloud of the input image. Then, we employ a neural Galerkin solver [Huang et al. 2022] to reconstruct the surface, forming a watertight mesh. Finally, the mesh is sent to a self-supervised SECAD-Net [Li et al. 2023] to predict the final CAD program.
- *DeepCAD*: We load the checkpoint of DeepCAD pretrained on the ABC dataset [Koch et al. 2019] and finetune it on our dataset. To enable image-to-CAD reconstruction, we follow the original approach in Wu et al. [2021], which involves a second-stage training to align the image encoder with the program encoder by minimizing the L2 loss over the latent vectors while keeping the decoder frozen.
- *DeepCAD-End2End*: We also include a variant of DeepCAD that jointly finetunes the image encoder and program decoder in an end-to-end manner. Empirically, we find this approach generally outperforms the naive DeepCAD, as it allows for the joint optimization of the image encoder and program decoder directly under the image-to-CAD prediction objective.

Evaluation metrics. We employ three metrics that cover both geometric and semantic proximity:

- *Chamfer Distance (CD)*: This is computed as the Chamfer distance between two point clouds uniformly sampled on the surface of the reconstructed mesh from the model-predicted CAD program and the ground truth.
- *Part Segmentation Accuracy (Seg Acc %)*: This measures how semantically close the reconstructed object is to the ground truth, specified as the part segmentation accuracy over the point cloud sampled on the surface.

Table 2: Ablation study on TrAssembler.

	Chair			Table			Cabinet		
	CD ↓	Seg Acc ↑	Seg mIoU ↑	CD ↓	Seg Acc ↑	Seg mIoU ↑	CD ↓	Seg Acc ↑	Seg mIoU ↑
Ours	0.1685	81.79	73.32	0.1655	83.75	69.55	0.2327	66.32	57.33
w/ Quantized Loss	0.1912	79.82	73.22	0.1881	81.77	67.40	0.3169	63.89	56.12
w/o Hierarchy	0.3282	64.64	49.90	0.2670	76.53	56.07	0.3013	62.99	54.77
w/o Semantics	0.2847	63.14	44.06	0.2645	49.10	32.17	0.2947	59.78	50.21

Table 3: Ablation study of GPT prompts on Chair test dataset.

Reminder	ContExample	CoT	Prog Succ ↑	CD ↓	Part IoU ↑
-	-	-	89.02	0.1601	59.82
✓	-	-	96.34	0.1388	68.22
✓	✓	-	98.78	0.1349	68.59
✓	✓	✓	98.78	0.1248	73.59

- *Part Segmentation mIoU* (Seg mIoU %): This metric also assesses semantic closeness, specified as the mean Intersection over Union (mIoU) of the part segmentation over the point cloud sampled on the surface. We leverage PointNet [Qi et al. 2017] pretrained on ShapeNet [Chang et al. 2015] to produce the segmentation from the generated CAD models. We then compare these segmentations with the ground-truth segmentation labels from ShapeNet to obtain Seg Acc and Seg mIoU. More details can be found in our supplementary material.

Main results. We present the image-to-CAD reconstruction results of our method against the baselines in Table 1. Qualitative results are illustrated in Figure 9. Img2CAD consistently outperforms the baselines across all three object categories and metrics, demonstrating its strong capability in producing both geometrically and structurally accurate CAD models from image inputs. Notably, Img2CAD reduces the Chamfer distance from 0.3698 to 0.1655 and improves segmentation accuracy and mIoU by 16.38% and 17.34%, respectively, over the best-performing baseline, DeepCAD-End2End, on the *Table* category.

The GPT-Only baseline performs significantly worse than the other approaches, validating that GPT-4V alone is insufficient to predict both the program structure and continuous attributes directly. This supports our approach of conditionally factorizing the task: using the program structure predicted by GPT-4V and offloading the attribute prediction to a learned network. Both DeepCAD and DeepCAD-End2End achieve better performance than GPT-Only but are still markedly inferior to Img2CAD.

Ablation on TrAssembler. We ablate several core designs of our TrAssembler with results depicted in Table 2 and qualitatively visualized in Figure 10. Note that these variants are all conditioned on the program structure predicted by GPT-4V.

We first implement a variant of TrAssembler that quantizes the continuous parameters into 256 bins, turning parameter fitting into a classification problem. This variant generally leads to slightly worse performance compared to TrAssembler, highlighting the advantage of directly predicting continuous values for CAD parameters. Notably, the variant of TrAssembler with quantized loss still

outperforms DeepCAD, showcasing the benefit of conditional factorization – i.e., using GPT-4V for discrete structure and a learned network for continuous parameters.

We further investigate the importance of using both (i) hierarchical transformer design and (ii) semantic part comment information in our TrAssembler. *w/o Hierarchy* removes the hierarchical design but retains the semantic labels. Specifically, it concatenates part label embeddings and command tokens into a 1D array that is fed through a single, flat transformer. This variant demonstrates how essential the hierarchical structure is for effectively capturing both local and global interactions within the CAD model, as the performance drops significantly without it. *w/o Semantics* keeps the hierarchical design but excludes the semantic part comments, showing that even with a robust hierarchical architecture, the absence of semantic information results in poorer performance.

These results, depicted in Table 2 and visualized in Figure 10, underscore the necessity of both the hierarchical transformer design and the inclusion of semantic part comments for optimal performance in TrAssembler.

Ablation studies on GPT-4V prompt. We further discuss the importance of three techniques we adopt in GPT-4V prompting:

- *Reminder:* We add several bullet-point reminders to ensure the CAD program is complete without missing any parts (e.g., "Give the FULL PROGRAM for ALL PARTS").
- *In-context Example (ContExample):* We provide GPT-4V with an example program for a chair’s backrest.
- *Chain of Thoughts (CoT):* We instruct GPT-4V to first enumerate all object parts in the image and then output programs for each part, rather than generating a single full program.

For this ablation, we use the oracle assembling process (discussed in Section 5) instead of TrAssembler to eliminate any confounding factors introduced by the assembling process. We report CD together with two additional metrics:

- *Program Success rate* (Prog Succ %): This reflects how effectively GPT-4V generates a valid CAD program.
- *Part IoU (%)*: This measures the consistency of GPT-generated semantic part labels with the ground-truth labels. Part IoU is computed by measuring the average frequency with which the predicted label and its corresponding ground-truth label have a CLIP embedding distance larger than 0.8.

The results of these ablation studies, detailed in Table 3, demonstrate the critical role of these prompting techniques in improving the quality and completeness of the generated CAD programs. The inclusion of reminders, in-context examples, and chain of thought reasoning significantly enhances both the program success rate and

Table 4: Our model achieves comparable performance on arbitrary views. Results are averaged over categories.

	CD ↓	Seg Acc ↑	Seg mIoU ↑
Frontal View	0.1889	77.29	66.73
Arbitrary View	0.1941	76.65	65.95

the part IoU, underscoring the necessity of these strategies for effective GPT-4V prompting. More details on these prompt modifications and metrics can be found in the supplementary materials.

Robustness on Arbitrary Viewpoints. Our method is also very robust thanks to the view invariance provided by large vision foundation models (i.e., GPT-4V and CLIP). As shown in Table 4, we achieve almost the same performance when evaluated on images sampled from arbitrary viewpoints. This important property helps make our method generalizable to images in the wild, even when it is trained on frontal-view images. Qualitative examples can be found in Figure 8.



Figure 8: Example output visualizations given arbitrary-viewpoint input images.

7 APPLICATIONS

7.1 Image To CAD in the Wild

Although our model is trained exclusively on synthetic ShapeNet CAD-ified models, it demonstrates the ability to generalize to real-world images. This is achieved through the foundational knowledge provided by vision language models such as GPT-4V and CLIP. Figures 11 and 12 present qualitative results using images from Pix3D [Sun et al. 2018] and Google product images, which offer an extensive collection of indoor furniture. It is important to note that this task is exceptionally challenging due to the difficulties associated with *generalization* and *CAD representation complexity*.

7.2 Structure-Aware Shape Editing in the Wild

A significant advantage of our method is its capability for structure-aware editing in real-world scenarios, enabled by our CAD representation. Figure 13 illustrates how users can easily modify the CAD structure of an object in an image, guided by natural language instructions. The process involves first obtaining the CAD program corresponding to the input image. Then, we feed this CAD program back to GPT, asking it to identify the key modifications needed to achieve the desired outcome. Users can make structural changes, such as adding an arc, or continuous attribute changes, such as editing the leg length, thereby creating variations easily from an

input image. This demonstrates the practical utility of our method for intuitive and precise CAD model editing.

8 CONCLUSION

We propose a novel approach for reverse engineering 3D CAD models from input images by conditionally factorizing this challenging task into two sub-problems. First, we leverage large foundation models (i.e., GPT-4V) to infer the discrete global structure with semantic information. We then introduce TrAssembler, which, conditioned on this discrete global structure, predicts the continuous attribute values of the CAD program. Additionally, we constructed a CAD dataset of common objects from ShapeNet to support the training of the continuous attribute prediction network. Our experiments demonstrate promising results, significantly outperforming previous baselines. Our method also makes a significant initial step towards generating CAD models from images in the wild, showcasing its potential for real-world applications.

Acknowledgements. This work is supported by ARL grant W911NF-21-2-0104, a Vannevar Bush Faculty Fellowship, and a Apple Scholars in AI/ML PhD Fellowship. Yang You is also supported in part by the Outstanding Doctoral Graduates Development Scholarship of Shanghai Jiao Tong University.

REFERENCES

- Josh Achiam, Steven Adler, Sandhini Agarwal, Lama Ahmad, Ilge Akkaya, Florencia Leoni Aleman, Diogo Almeida, Janko Altmenschmidt, Sam Altman, Shyamal Anadkat, et al. 2023. Gpt-4 technical report. *arXiv preprint arXiv:2303.08774* (2023).
- Jean-Baptiste Alayrac, Jeff Donahue, Pauline Luc, Antoine Miech, Iain Barr, Yana Hasson, Karel Lenc, Arthur Mensch, Katherine Millican, Malcolm Reynolds, et al. 2022. Flamingo: a visual language model for few-shot learning. *Advances in neural information processing systems* 35 (2022), 23716–23736.
- Autodesk. 2021. Fusion 360: 3D CAD, CAM, CAE & PCB Cloud-based software. <https://www.autodesk.co.uk/products/fusion-360/overview>
- Pál Benkő, Géza Kós, Tamás Várady, László Andor, and Ralph Robert Martin. 2002. Constrained fitting in reverse engineering. *Comput. Aided Geom. Des.* (2002).
- Pal Benko and Tamas Várady. 2004. Segmentation methods for smooth point regions of conventional engineering objects. *Computer-Aided Design* (2004).
- Dorit Borrmann, Jan Elseberg, Kai Lingemann, and Andreas Nüchter. 2011. The 3d hough transform for plane detection in point clouds: A review and a new accumulator design. *3D Research* 2 (2011).
- Francesco Buonamici, Monica Carfagni, Rocco Furferi, Lapo Governi, Alessandro Lapini, and Yary Volpe. 2018. Reverse engineering modeling methods and tools: a survey. *Computer-Aided Design and Applications* 15, 3 (2018), 443–464. <https://doi.org/10.1080/16864360.2017.1397894> arXiv:<https://doi.org/10.1080/16864360.2017.1397894>
- Rainer Burkard, Mauro Dell’Amico, and Silvano Martello. 2012. *Assignment problems: revised reprint*. SIAM.
- Roseline Bénéière, Gérard Subsol, Gilles Gesquière, François Le Breton, and William Puech. 2013. A comprehensive process of reverse engineering from 3D meshes to CAD models. *Computer-Aided Design* (2013).
- Cappgemini. [n. d.]. Open cascade technology. <https://www.opencascade.com/opencascade-technology/>
- Angel X Chang, Thomas Funkhouser, Leonidas Guibas, Pat Hanrahan, Qixing Huang, Zimo Li, Silvio Savarese, Manolis Savva, Shuran Song, Hao Su, et al. 2015. Shapenet: An information-rich 3d model repository. *arXiv preprint arXiv:1512.03012* (2015).
- Siddhartha Chaudhuri, Evangelos Kalogerakis, Leonidas Guibas, and Vladlen Koltun. 2011. Probabilistic Reasoning for Assembly-Based 3D Modeling. *ACM Transactions on Graphics (Proc. SIGGRAPH)* (2011).
- Justin Curry. 2014. Sheaves, Cosheaves and Applications. arXiv:1303.3255 [math.AT]
- T Czerniawski, B Sankaran, M Nahangi, C Haas, and F Leite. 2018. 6D DBSCAN-based segmentation of building point clouds for planar object classification. *Automation in Construction* 88 (2018), 44–58.
- Bertram Drost and Slobodan Ilic. 2015. Local hough transform for 3d primitive detection. In *3DV*.
- Tao Du, Jeevana Priya Inala, Yewen Pu, Andrew Spielberg, Adriana Schulz, Daniela Rus, Armando Solar-Lezama, and Wojciech Matusik. 2018. InverseCSG: Automatic Conversion of 3D Models to CSG Trees. *ACM Transactions on Graphics (TOG)* (2018).

- Elona Dupont, Kseniya Cherenkova, Anis Kacem, Sk Aziz Ali, Ilya Arzhannikov, Gleb Gusev, and Djamila Aouada. 2022. CADOps-Net: Jointly Learning CAD Operation Types and Steps from Boundary-Representations. In *3DV*.
- Hao Fang, Florent Lafarge, and Mathieu Desbrun. 2018. Planar Shape Detection at Structural Scales. In *IEEE Conference on Computer Vision and Pattern Recognition (CVPR)*.
- Martin A Fischler and Robert C Bolles. 1981. Random sample consensus: a paradigm for model fitting with applications to image analysis and automated cartography. *Commun. ACM* 24, 6 (1981), 381–395.
- Vignesh Ganapathi-Subramanian, Olga Diamanti, Sören Pirk, Chengcheng Tang, Matthias Nießner, and Leonidas J. Guibas. 2018. Parsing Geometry Using Structure-Aware Shape Templates. *2018 International Conference on 3D Vision (3DV)* (2018), 672–681. <https://api.semanticscholar.org/CorpusID:51926351>
- Yaroslav Ganin, Sergey Bartunov, Yujia Li, Ethan Keller, and Stefano Saliceti. 2021. Computer-Aided Design as Language. In *NeurIPS*.
- Haoxiang Guo, Shilin Liu, Hao Pan, Yang Liu, Xin Tong, and Baining Guo. 2022. ComplexGen: CAD Reconstruction by B-Rep Chain Complex Generation. In *SIGGRAPH*.
- Jiahui Huang, Hao-Xiang Chen, and Shi-Min Hu. 2022. A neural galerkin solver for accurate surface reconstruction. *ACM Transactions on Graphics (TOG)* 41, 6 (2022), 1–16.
- Pradeep Kumar Jayaraman, Joseph G. Lambourne, Nishkrit Desai, Karl D. D. Willis, Aditya Sanghi, and Nigel J. W. Morris. 2023. SolidGen: An Autoregressive Model for Direct B-rep Synthesis. [arXiv:2203.13944](https://arxiv.org/abs/2203.13944) [cs.LG]
- Pradeep Kumar Jayaraman, Aditya Sanghi, Joseph G. Lambourne, Karl D.D. Willis, Thomas Davies, Hooman Shayani, and Nigel Morris. 2021. UV-Net: Learning from Boundary Representations. In *CVPR*.
- R. Kenny Jones, Theresa Barton, Xianghao Xu, Kai Wang, Ellen Jiang, Paul Guerrero, Niloy Mitra, and Daniel Ritchie. 2020. ShapeAssembly: Learning to Generate Programs for 3D Shape Structure Synthesis. *ACM Transactions on Graphics (TOG), Siggraph Asia 2020* 39, 6 (2020), Article 234.
- R. Kenny Jones, David Charatan, Paul Guerrero, Niloy J. Mitra, and Daniel Ritchie. 2021. ShapeMOD: Macro Operation Discovery for 3D Shape Programs. *ACM Transactions on Graphics (TOG)* 40, 4, Article 153 (2021).
- R. Kenny Jones, Paul Guerrero, Niloy J. Mitra, and Daniel Ritchie. 2023. ShapeCoder: Discovering Abstractions for Visual Programs from Unstructured Primitives. *ACM Transactions on Graphics (TOG), Siggraph 2023* 42, 4, Article 49 (2023).
- Evangelos Kalogerakis, Siddhartha Chaudhuri, Daphne Koller, and Vladlen Koltun. 2012. A probabilistic model for component-based shape synthesis. *ACM Trans. Graph.*, Article 55 (jul 2012), 11 pages.
- Kacper Kania, Maciej Zięba, and Tomasz Kajdanowicz. 2020. UCSG-Net – Unsupervised Discovering of Constructive Solid Geometry Tree. In *NeurIPS*.
- Mohammad Sadil Khan, Elona Dupont, Sk Aziz Ali, Kseniya Cherenkova, Anis Kacem, and Djamila Aouada. 2024. CAD-SIGNet: CAD Language Inference from Point Clouds using Layer-wise Sketch Instance Guided Attention. [arXiv:2402.17678](https://arxiv.org/abs/2402.17678) [cs.CV]
- Vladimir G. Kim, Wilmot Li, Niloy J. Mitra, Siddhartha Chaudhuri, Stephen DiVerdi, and Thomas Funkhouser. 2013. Learning Part-based Templates from Large Collections of 3D Shapes. *ACM Transactions on Graphics (Proc. SIGGRAPH)* 32, 4 (July 2013).
- Sebastian Koch, Albert Matveev, Zhongshi Jiang, Francis Williams, Alexey Artemov, Evgeny Burnaev, Marc Alexa, Denis Zorin, and Daniele Panozzo. 2019. Abc: A big cad model dataset for geometric deep learning. In *Proceedings of the IEEE/CVF conference on computer vision and pattern recognition*. 9601–9611.
- Milin Kodonogbua, Benjamin T. Jones, Maaz Bin Safeer Ahmad, Vladimir Kim, and Adriana Schulz. 2023. ReParamCAD: Zero-shot CAD Re-Parameterization for Interactive Manipulation. *SIGGRAPH Asia 2023 Conference Papers* (2023). <https://api.semanticscholar.org/CorpusID:266177414>
- Joseph George Lambourne, Karl Willis, Pradeep Kumar Jayaraman, Longfei Zhang, Aditya Sanghi, and Kamal Rahimi Malekshan. 2022. Reconstructing editable prismatic CAD from rounded voxel models. In *SIGGRAPH Asia 2022 Conference Papers (SA '22)*.
- Joseph G. Lambourne, Karl D. D. Willis, Pradeep Kumar Jayaraman, Aditya Sanghi, Peter Meltzer, and Hooman Shayani. 2021. BRepNet: A topological message passing system for solid models. In *CVPR*.
- Eric-Tuan Lê, Minhuk Sung, Duygu Ceylan, Radomir Mech, Tamy Boubekeur, and Niloy J. Mitra. 2021. CFPN: Cascaded Primitive Fitting Networks for High-Resolution Point Clouds. In *ICCV*.
- Jun Li, Kai Xu, Siddhartha Chaudhuri, Ersin Yumer, Hao Zhang, and Leonidas Guibas. 2017. GRASS: Generative Recursive Autoencoders for Shape Structures. *ACM Transactions on Graphics (Proc. of SIGGRAPH 2017)* 36, 4 (2017), to appear.
- Lingxiao Li, Minhuk Sung, Anastasia Dubrovina, Li Yi, and Leonidas Guibas. 2019. Supervised Fitting of Geometric Primitives to 3D Point Clouds. In *CVPR*.
- Pu Li, Jianwei Guo, Xiaopeng Zhang, and Dong-Ming Yan. 2023. SECAD-Net: Self-Supervised CAD Reconstruction by Learning Sketch-Extrude Operations. In *CVPR*.
- Yanyan Li, Xiaokun Wu, Yiorgos Chrysathou, Andrei Sharf, Daniel Cohen-Or, and Niloy J. Mitra. 2011. Globfit: Consistently fitting primitives by discovering global relations. In *ACM Transactions on Graphics (TOG)*.
- Yujia Liu, Anton Obukhov, Jan Dirk Wegner, and Konrad Schindler. 2023. Point2CAD: Reverse Engineering CAD Models from 3D Point Clouds. [arXiv:2312.04962](https://arxiv.org/abs/2312.04962) [cs.CV]
- Weijian Ma, Minyang Xu, Xueyang Li, and Xiangdong Zhou. 2023. MultiCAD: Contrastive Representation Learning for Multi-modal 3D Computer-Aided Design Models. *Proceedings of the 32nd ACM International Conference on Information and Knowledge Management* (2023).
- N. J. Mitra, L. Guibas, and M. Pauly. 2006. Partial and Approximate Symmetry Detection for 3D Geometry. *ACM Transactions on Graphics (SIGGRAPH)* 25, 3 (2006), 560–568.
- Kaichun Mo, Paul Guerrero, Li Yi, Hao Su, Peter Wonka, Niloy Mitra, and Leonidas Guibas. 2019a. StructureNet: Hierarchical Graph Networks for 3D Shape Generation. *ACM Transactions on Graphics (TOG), Siggraph Asia 2019* 38, 6 (2019), Article 242.
- Kaichun Mo, Shilin Zhu, Angel X Chang, Li Yi, Subarna Tripathi, Leonidas J Guibas, and Hao Su. 2019b. Partnet: A large-scale benchmark for fine-grained and hierarchical part-level 3d object understanding. In *Proceedings of the IEEE/CVF conference on computer vision and pattern recognition*. 909–918.
- Aron Monszpart, Nicolas Mellado, Gabriel J Brostow, and Niloy J Mitra. 2015. RAPter: rebuilding man-made scenes with regular arrangements of planes. *ACM Transactions on Graphics (TOG)* (2015).
- Pascal Müller, Peter Wonka, Simon Haegler, Andreas Ulmer, and Luc Van Gool. 2023. *Procedural Modeling of Buildings*.
- Alex Nichol, Heewoo Jun, Pratul Dharwal, Pamela Mishkin, and Mark Chen. 2022. Point-e: A system for generating 3d point clouds from complex prompts. [arXiv preprint arXiv:2212.08751](https://arxiv.org/abs/2212.08751) (2022).
- Sven Oesau, Florent Lafarge, and Pierre Alliez. 2016. Planar shape detection and regularization in tandem. In *Computer Graphics Forum*.
- Maks Ovsjanikov, Wilmot Li, Leonidas Guibas, and Niloy J. Mitra. 2011. Exploration of Continuous Variability in Collections of 3D Shapes. *ACM Transactions on Graphics* 30, 4 (2011), to appear.
- Wamiq Reyaz Para, Shariq Farooq Bhat, Paul Guerrero, Tom Kelly, Niloy Mitra, Leonidas Guibas, and Peter Wonka. 2021. SketchGen: Generating Constrained CAD Sketches. (2021).
- Despoina Paschalidou, Ali Osman Ulusoy, and Andreas Geiger. 2019. Superquadrics Revisited: Learning 3D Shape Parsing beyond Cuboids. In *Proceedings IEEE Conf. on Computer Vision and Pattern Recognition (CVPR)*.
- Despoina Paschalidou, Luc van Gool, and Andreas Geiger. 2020. Learning Unsupervised Hierarchical Part Decomposition of 3D Objects from a Single RGB Image. In *Proceedings IEEE Conf. on Computer Vision and Pattern Recognition (CVPR)*.
- Charles R Qi, Hao Su, Kaichun Mo, and Leonidas J Guibas. 2017. Pointnet: Deep learning on point sets for 3d classification and segmentation. In *Proceedings of the IEEE conference on computer vision and pattern recognition*. 652–660.
- Alec Radford, Jong Wook Kim, Chris Hallacy, Aditya Ramesh, Gabriel Goh, Sandhini Agarwal, Girish Sastry, Amanda Askell, Pamela Mishkin, Jack Clark, et al. 2021. Learning transferable visual models from natural language supervision. In *International conference on machine learning*. PMLR, 8748–8763.
- Daxuan Ren, Jianmin Zheng, Jianfei Cai, Jiatong Li, Haiyong Jiang, Zhongang Cai, Junzhe Zhang, Liang Pan, Mingyuan Zhang, Haiyu Zhao, and Shuai Yi. 2021. CSG-Stump: A Learning Friendly CSG-Like Representation for Interpretable Shape Parsing. In *ICCV*.
- Daxuan Ren, Jianmin Zheng, Jianfei Cai, Jiatong Li, and Junzhe Zhang. 2022. ExtrudeNet: Unsupervised inverse sketch-and-extrude for shape parsing. In *ECCV*.
- Daniel Ritchie, Paul Guerrero, R. Kenny Jones, Niloy J. Mitra, Adriana Schulz, Karl D. D. Willis, and Jiajun Wu. 2023. Neurosymbolic Models for Computer Graphics. [arXiv:2304.10320](https://arxiv.org/abs/2304.10320) [cs.GR]
- Ruwen Schnabel, Roland Wahl, and Reinhard Klein. 2007. Efficient RANSAC for point-cloud shape detection. In *Computer graphics forum*.
- Ari Seff, Yaniv Ovadia, Wenda Zhou, and Ryan P. Adams. 2020. SketchGraphs: A Large-Scale Dataset for Modeling Relational Geometry in Computer-Aided Design. In *ICML*.
- Gopal Sharma, Rishabh Goyal, Difan Liu, Evangelos Kalogerakis, and Subhransu Maji. 2018. CSGNet: Neural Shape Parser for Constructive Solid Geometry. In *CVPR*.
- Gopal Sharma, Difan Liu, Evangelos Kalogerakis, Subhransu Maji, Siddhartha Chaudhuri, and Radomir Méch. 2020. ParSeNet: A Parametric Surface Fitting Network for 3D Point Clouds. In *ECCV*.
- Xingyuan Sun, Jiajun Wu, Xiuming Zhang, Zhoutong Zhang, Chengkai Zhang, Tianfan Xue, Joshua B Tenenbaum, and William T Freeman. 2018. Pix3d: Dataset and methods for single-image 3d shape modeling. In *Proceedings of the IEEE conference on computer vision and pattern recognition*. 2974–2983.
- Minhyuk Sung, Zhenyu Jiang, Panos Achlioptas, Niloy J. Mitra, and Leonidas J. Guibas. 2020. DeformSyncNet: Deformation Transfer via Synchronized Shape Deformation Spaces. *ACM Transactions on Graphics (Proc. of SIGGRAPH Asia)* (2020).
- Minhyuk Sung, Vladimir G. Kim, Roland Angst, and Leonidas Guibas. 2015. Data-driven Structural Priors for Shape Completion. *ACM Transactions on Graphics (Proc. of SIGGRAPH Asia)* (2015).
- Dassault Systèmes. 2005. SolidWorks®. *Version Solidworks* (2005).
- Shubham Tulsiani, Hao Su, Leonidas J. Guibas, Alexei A. Efros, and Jitendra Malik. 2017. Learning Shape Abstractions by Assembling Volumetric Primitives. In *CVPR*.
- Mikaela Angelina Uy, Yen-Yu Chang, Minhuk Sung, Purvi Goel, Joseph G Lambourne, Tolga Birdal, and Leonidas J Guibas. 2022. Point2cyl: Reverse engineering 3d objects from point clouds to extrusion cylinders. In *CVPR*. 11850–11860.

- Mikaela Angelina Uy, Jingwei Huang, Minhyuk Sung, Tolga Birdal, and Leonidas Guibas. 2020. Deformation-Aware 3D Model Embedding and Retrieval. In *European Conference on Computer Vision (ECCV)*.
- Mikaela Angelina Uy, Vladimir G. Kim, Minhyuk Sung, Noam Aigerman, Siddhartha Chaudhuri, and Leonidas Guibas. 2021. Joint Learning of 3D Shape Retrieval and Deformation. In *IEEE Conference on Computer Vision and Pattern Recognition (CVPR)*.
- Tamás Várady, Ralph R Martin, and Jordan Cox. 1997. Reverse engineering of geometric models—an introduction. *Computer-Aided Design* (1997).
- Jason Wei, Xuezhi Wang, Dale Schuurmans, Maarten Bosma, Fei Xia, Ed Chi, Quoc V Le, Denny Zhou, et al. 2022. Chain-of-thought prompting elicits reasoning in large language models. *Advances in neural information processing systems* 35 (2022), 24824–24837.
- Karl DD Willis, Yewen Pu, Jieliang Luo, Hang Chu, Tao Du, Joseph G Lambourne, Armando Solar-Lezama, and Wojciech Matusik. 2021. Fusion 360 gallery: A dataset and environment for programmatic cad construction from human design sequences. *ACM Transactions on Graphics (TOG)* (2021).
- Rundi Wu, Chang Xiao, and Changxi Zheng. 2021. DeepCAD: A Deep Generative Network for Computer-Aided Design Models. In *ICCV*.
- Xiang Xu, Pradeep Kumar Jayaraman, Joseph G Lambourne, Karl DD Willis, and Yasutaka Furukawa. 2023. Hierarchical Neural Coding for Controllable CAD Model Generation. *arXiv preprint arXiv:2307.00149* (2023).
- Xiang Xu, Karl DD Willis, Joseph G Lambourne, Chin-Yi Cheng, Pradeep Kumar Jayaraman, and Yasutaka Furukawa. 2022. SkexGen: Autoregressive Generation of CAD Construction Sequences with Disentangled Codebooks. In *ICML*.
- Fenggen Yu, Qimin Chen, Maham Tanveer, Ali Mahdavi Amiri, and Hao Zhang. 2023. D²CSG: Unsupervised Learning of Compact CSG Trees with Dual Complements and Dropouts. In *NeurIPS*.
- Shuming Zhang, Zhidong Guan, Hao Jiang, Tao Ning, Xiaodong Wang, and Pingan Tan. 2024. Brep2Seq: a dataset and hierarchical deep learning network for reconstruction and generation of computer-aided design models. *Journal of Computational Design and Engineering* (2024).
- Chuhang Zou, Ersin Yumer, Jimei Yang, Duygu Ceylan, and Derek Hoiem. 2017. 3d-prnn: Generating shape primitives with recurrent neural networks. In *ICCV*.



Figure 9: Qualitative results between different methods on the test split of ShapeNet CAD-ified dataset. Our method achieves much better results.



Figure 10: Qualitative comparisons of our ablation studies.



Figure 11: Image2CAD results on Pix3D dataset.



Figure 12: Image2CAD results on google product images.

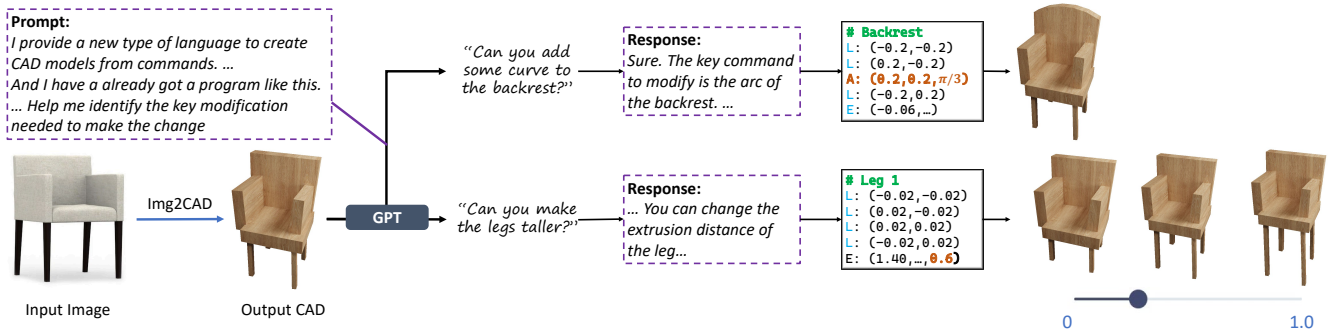


Figure 13: Image conditioned CAD editing example. Users can easily create multiple variations of a target object from a single-view image.

APPENDIX

A.1 Experiment Details

A.1.1 Sketch and Extrusion Command Details. In our experiments, to ensure compatibility with the OpenCasCade [Cappemini [n. d.]] library, we always append the *OneSided* indicator after the extrusion command, as we only consider one-sided extrusion. Additionally, there is a clockwise/counter-clockwise flag for the *arc* command, which we always set to 1, as our sketches are always drawn in a counter-clockwise order.

A.1.2 GPT Prompt. We use the following text as the inference prompt for GPT-4V. For clarity, we also add explanations of the role of each section of the prompt as comments, all marked in red (these comments are not part of the prompt). In the comments, we also specify the paragraphs that correspond to *Reminder*, *ContExample*, and *CoT* used in our ablation studies in Table 4.

Basic rules of a sketch-extrude CAD program

I provide a new type of language to create CAD models from commands. The command has two types: sketch and extrude.

Sketch commands are used to specify closed curves on a 2D plane in 3D space. Primarily, we consider closed curves which are formed from concatenations of LINES, ARCS, and CIRCLES.

In our representation, a PROFILE is a list which starts with an indicator command $\langle SOL \rangle$, followed by a series of curve commands C_i (which are lines, arcs, or circles). There are four important requirements in creating our sketch profile. 1) The first curve starts at the ORIGIN. 2) The last curve ends at the ORIGIN. 3) The end of each curve is the start of the next curve. 4) The sketch should be drawn in COUNTERCLOCKWISE order.

Each curve command C_i is described by its curve type $t_i \in \langle SOL \rangle, L, A, R$, where L is specified in (x, y) format giving the next line end-point, A is in (x, y, α, f) giving the next arc end-point, sweep angle α and counter-clockwise flag f (0 clockwise, 1 counter-clockwise), R is in (x, y, r) representing the center (x, y) and the radius r .

Extrude commands have two purposes. 1) It extrudes a sketch profile from a 2D plane into a 3D body with one-sided extrusion. 2) The command also specifies how to merge newly extruded 3D body with the previously created shape, using *NewBody*. Extrude commands are in the following format: $(n_x, n_y, n_z, x, y, z, e, b, u)$, where n_x, n_y, n_z represent the 2D plane's orientation (normal) in 3D space. x, y, z are the location of the plane's origin, e is the one-sided extrusion distance. The extrusion distance gives the HEIGHT or THICKNESS of the extruded profile ALONG THE EXTRUSION AXIS DIRECTION. b is the boolean type which should be *NewBody*, u is the extrusion type which should be *OneSided*.

It is also important to note the COORDINATE SYSTEM CONVENTION of the program outputs. The COORDINATE SYSTEM CONVENTION is given as the Z-AXIS is the gravity axis pointing DOWNWARDS, the X-AXIS points OUTWARDS, and the Y-AXIS points TO THE RIGHT.

A CAD program example on cubes

For example, to create three cubes of side length 2 units placed horizontally in the x direction (with a space of 3 units between corresponding corners of adjacent cubes), we could use the following program:

```
<SOL>
L: (2,0)
L: (2,2)
L: (0,2)
L: (0,0)
E: (0,0,1,0,0,0,2,NewBody,OneSided)
<SOL>
L: (2,0)
L: (2,2)
L: (0,2)
L: (0,0)
E: (0,0,1,3,0,0,2,NewBody,OneSided)
<SOL>
L: (2,0)
L: (2,2)
L: (0,2)
L: (0,0)
E: (0,0,1,6,0,0,2,NewBody,OneSided)
```

Note how here, we also make sure to draw the sketches in COUNTERCLOCKWISE order. Moreover we see that the cubes are extruded along the z-axis, the gravity axis.

Since cuts are not covered by the above commands, there is a separate syntax to form cuts. If you want to cut out of a base sketch, you should insert <CUT> followed by the sketch (in the same syntax as above for usual sketches) you wish to cut out of the base sketch. The coordinates will be in the same frame. YOU MUST PLACE THIS CUT BLOCK AFTER THE SKETCH COMMANDS FOR THE BASE SKETCH, BUT BEFORE THE EXTRUDE COMMAND FOR THE BASE SKETCH.

IT'S ALSO IMPORTANT TO RECOGNIZE CURVES WHEN THEY ARISE IN SKETCHES, AND CREATE THEM WITH ARC COMMANDS. Arc commands can be useful when we wish to create curves.

The in-context example for chair (ContExample in Table 4)

This is the corresponding program to create a chair backrest with an arc using the arc command (A) as well as a circular hole with the CUT and R command.

```
<SOL>
L: (3,0)
L: (3,5)
A: (0,5,120,1)
L: (0,0)
<CUT>
R: (1.5,2,1)
E: (-1,0,0,0,0,-0.5,NewBody,OneSided)
```

Remember the L:(0,0) is to close the loop, and that the non-cut sketch loop is drawn counterclockwise. Also note here that we made the cut radius equal to 1 to keep the cut within the scope of the original sketch. The angle 120 in the 'A:' command denotes the angle formed by the arc in degrees, and the 1 indicates the counterclockwise flag direction (SAME AS THE COUNTERCLOCKWISE SKETCH DIRECTION!).

Note that in this example the backrest was extruded in the X-axis which points outwards, to define the thickness of the backrest. This is different from the natural extrusion axis direction of the chair leg which is typically the z-axis to capture different chair heights.

The reminder of the basic rules (Reminder in Table 4)

Now, using this language, produce a sequence of commands to form the following 3D rendering of the model. Keep the following three rules in mind: 1. It is VERY IMPORTANT to detect and reconstruct ALL PARTS of the object in the given image. So please DO NOT MISS ANY PARTS. Please pay attention and be careful. 2. COMMENT PARTS with DISTINCT LABELS in the code. If a part is repeated (like a leg), please give DISTINCT COMMENTS WITH NUMBERS (LIKE #LEG 1, #LEG 2, ETC.). 3. Give the FULL PROGRAM for ALL PARTS. EXPLICITLY WRITE OUT the program line by line. Do NOT say or use words like "REPEAT", "FOLLOWING THE PATTERN", ELLIPSIS "...". It is IMPORTANT TO WRITE OUT THE FULL PROGRAM. 4. Follow the coordinate system convention as given when creating the shapes, and PROVIDE AN EXPLANATION FOR THE EXTRUSION AXIS FOR EACH PART IN RELATION TO THE COORDINATE SYSTEM CONVENTION. Moreover, give its thickness. 5. Provide a description of the shape of the sketch in the comments.

Chain-of-Thought prompting by asking GPT to enumerate all parts then write the program (CoT in Table 4)

Can you first enumerate all the parts that you see in the chair in the given image and then give me the corresponding FULL program for it?

A.1.3 Implementation Details of Img2CAD and TrAssembler. The embedding size for all q , k , and v in our transformers is 256. Each transformer comprises a layer normalization, an 8-head self-attention layer, and three fully connected layers with a dimension of 256. For the part transformer encoder, we additionally concatenate the positional encoding with the input command tokens to distinguish the order of different commands within each part. We utilize the pretrained CLIP model with the ViT-B/32 architecture to encode the text label and the input image.

For multiple extrusions in the same part, e.g., two extrusions within a cut backrest (one for the outer sketch and the other for the inner cut), we concatenate them into the same block under the same part label. For different parts with the same label, such as two legs, we further sort these parts using their ground-truth bounding box center and concatenate a positional embedding after sorting. This ensures that the global transformer has sufficient information to distinguish between different legs and outputs different attribute parameters for each.

We use a batch size of 64 and a learning rate of 3×10^{-4} with a weight decay of 1×10^{-6} . For each category, we train TrAssembler for 300 epochs.

A.1.4 Detailed Implementation of the Baselines.

DeepCAD and DeepCAD-End2End. For both DeepCAD and DeepCAD-End2End, the image encoder is instantiated similarly to our Img2CAD model. This encoder includes a CLIP embedding module with a ViT-B/32 architecture and a Multi-Layer Perceptron (MLP) with 6 layers, ReLU activation, and a hidden dimension of 256. To adapt the original point cloud-conditioned DeepCAD from Wu et al. [2021] to an

Table A1: Detailed statistics of our dataset. The total number of data points (Size) and the maximum/average number of lines and parts are exhibited.

Chair			Table			Cabinet		
Size	Max/Ave # Lines	Max/Ave # Parts	Size	Max/Ave # Lines	Max/Ave # Parts	Size	Max/Ave # Lines	Max/Ave # Parts
1026	107/58.14	15/9.44	3243	99/48.44	15/8.06	305	110/62.94	15/10.28

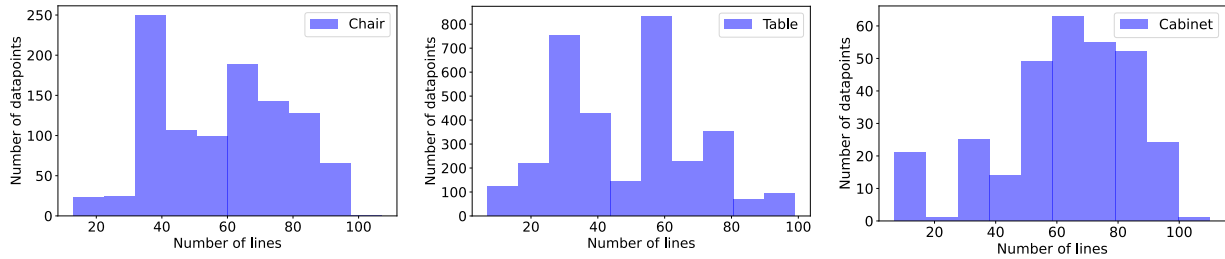


Figure A1: The distribution of the number of lines (top) and the number of parts (bottom) in the CAD program of our dataset.

image-conditioned model, we replace the point cloud encoder with the image encoder. The model is initially fine-tuned on our dataset using an auto-encoding objective. Subsequently, the program encoder and decoder are frozen, and the image encoder is optimized to minimize the L2 distance between the vectors embedded by the program encoder and the image encoder, given the program-image pairs as input. For DeepCAD-End2End, both the image encoder and program decoder are optimized by minimizing the cross-entropy loss on the commands and the quantized bins of the parameters.

A.1.5 Detailed Implementation of Our Ablations. For the quantized version of Img2CAD discussed in Table 2, we follow DeepCAD by quantizing the continuous parameter space into 256 bins. We modify the final output head of our model to be a classifier with an output dimension of 256, and the input encoding layer for the parameters to be a learnable embedding dictionary with a vocabulary size of 256. All other components are kept the same as in the original Img2CAD model.

A.1.6 Details in Computing the Metrics. For our main results, we adopt Chamfer Distance (CD), Part Segmentation Accuracy (Seg Acc), and Part Segmentation mean Intersection over Union (Seg mIoU) as the metrics. Specifically, for Chamfer Distance, we first reconstruct the 3D mesh using the model-predicted CAD program and uniformly sample 8,000 points on the surface of the mesh. Similarly, we sample 8,000 points on the surface of the ground truth mesh, reconstructed from the ground truth CAD program in our test set. The Chamfer Distance is then computed as the average distance between these two point clouds over all points.

For segmentation metrics, we use the part segmentation labels from ShapeNet. After obtaining the point cloud sampled from the reconstructed mesh, we assign a part label to each point in the point cloud based on the label of its nearest neighbor in the point cloud of the same ShapeNet model. Segmentation Accuracy (Seg Acc) and mean Intersection over Union (Seg mIoU) are then computed using a PointNet pretrained on the ShapeNet part segmentation task as the segmentation network.

A.1.7 More Details on Dataset. We present the detailed statistics of our dataset, including the number of data points, and the maximum and average number of lines and parts in the CAD program, in Table A1. Additionally, we plot the distribution of the number of lines and parts across all three datasets in Figure A1. As shown in the statistics, our dataset provides a detailed semantic description of common objects with a large number of semantic parts. Moreover, our dataset is more challenging, with significantly more lines in the CAD program compared to the previous CAD dataset ABC [Koch et al. 2019]. We also follow the split of PartNet [Mo et al. 2019b] for our dataset, resulting in 862/164, 2691/552, and 252/53 training/testing data points for chairs, tables, and cabinets, respectively.

A.2 More Experiment Results

A.2.1 Detailed Results of DeepCAD-AE. We provide the auto-encoding fitting results of DeepCAD-AE and DeepCAD-AE fine-tuned on our dataset with all three metrics (CD, Seg Acc, and Seg mIoU) in Table A2. For these two models, the input is our CAD-ified 3D point cloud and the output is the same point cloud, as suggested by the term "auto-encoding." Fine-tuning on our dataset improves the performance of DeepCAD on the CAD representation of common objects, including chairs, tables, and cabinets, highlighting the value of our curated dataset. It illustrates that the pretrained DeepCAD, trained only on the ABC dataset [Koch et al. 2019], struggles to understand domestic common objects. However, it can achieve better performance when fine-tuned on our introduced CAD-ified data of everyday common objects, which supports the usability of our dataset to supplement the existing ABC dataset [Koch et al. 2019], which focuses on industrial parts.

Table A2: DeepCAD auto-encoder fitting results on the test split of our dataset. We report Chamfer Distance (CD), Part Segmentation Accuracy (Seg Acc) and Part Segmentation mIoU (Seg mIoU) on all three categories. Fine-tuning on our dataset consistently improves all three metrics.

	Chair			Table			Cabinet		
	CD ↓	Seg Acc ↑	Seg mIoU ↑	CD ↓	Seg Acc ↑	Seg mIoU ↑	CD ↓	Seg Acc ↑	Seg mIoU ↑
DeepCAD-AE	0.4015	34.05	30.58	0.4054	44.22	30.34	0.3799	55.86	43.96
DeepCAD-AE-finetuned	0.2101	74.96	64.46	0.2031	77.35	63.96	0.3109	65.86	52.91

A.2.2 More Ablations on Conditional Structure Factorization. We propose using a nearest neighbor approach to retrieve the semantic labels of each part at inference time. Specifically, at inference time, we parse the GPT-4V’s output and extract the semantics as the text comments GPT-4V produces at the beginning of the CAD program for each part. Empirically, however, the semantics provided by GPT-4V can be noisy. To stabilize the semantic embeddings, we replace the inferred semantics with the nearest neighbor from the set of semantics that appear in our training set. The distance between semantics is measured by the L2 distance between their CLIP embeddings. We refer to this approach as GPT w/ Retrieval.

Since our model is trained on the CLIP embeddings of the semantics, it also generalizes well without retrieval, which we refer to as GPT w/o Retrieval. As shown in Table A3, for both Img2CAD and its quantized version, the retrieval procedure generally improves performance, especially on the semantic segmentation metrics, such as Seg Acc and Seg mIoU. Moreover, our model without retrieval still outperforms the baselines, such as DeepCAD-End2End, by a significant margin. This is because we embed the semantic labels using a pretrained CLIP model, which can generalize to unseen texts appearing at inference time.

Table A3: Ablation studies on semantics acquisition in conditional structure factorization. Performing nearest neighbor retrieval for the GPT output leads to performance increase especially on the semantic segmentation metrics, for both Img2CAD and its quantized version.

Quantized	Semantics Acquisition	Chair			Table			Cabinet		
		CD ↓	Seg Acc ↑	Seg mIoU ↑	CD ↓	Seg Acc ↑	Seg mIoU ↑	CD ↓	Seg Acc ↑	Seg mIoU ↑
-	GPT w/ Retrieval	0.1685	81.79	73.32	0.1655	83.75	69.55	0.2327	66.32	57.33
-	GPT w/o Retrieval	0.1866	78.27	68.41	0.1691	82.58	67.56	0.2291	65.06	55.30
✓	GPT w/ Retrieval	0.1912	79.82	73.22	0.1881	81.77	67.40	0.3169	63.89	56.12
✓	GPT w/o Retrieval	0.2116	74.55	64.14	0.2035	78.99	63.95	0.2894	67.94	54.38

A.3 Additional Qualitative Results

We further include additional qualitative results. Figure A2 shows additional examples for our ablation study, while Figure A3 shows additional real world examples on the Pix3D dataset.

A.4 Dataset Visualization

We include visualizations of some examples of our CAD dataset of common everyday objects as shown in Figure A4, A5, A6.



Figure A2: Additional qualitative comparisons of ablation studies on ShapeNet CAD-ified test set.



Figure A3: Additional Image to CAD results on Pix3D dataset.



Figure A4: Dataset visualizations for chairs. For each pair, left: ShapeNet model, right: our CAD-ified model.

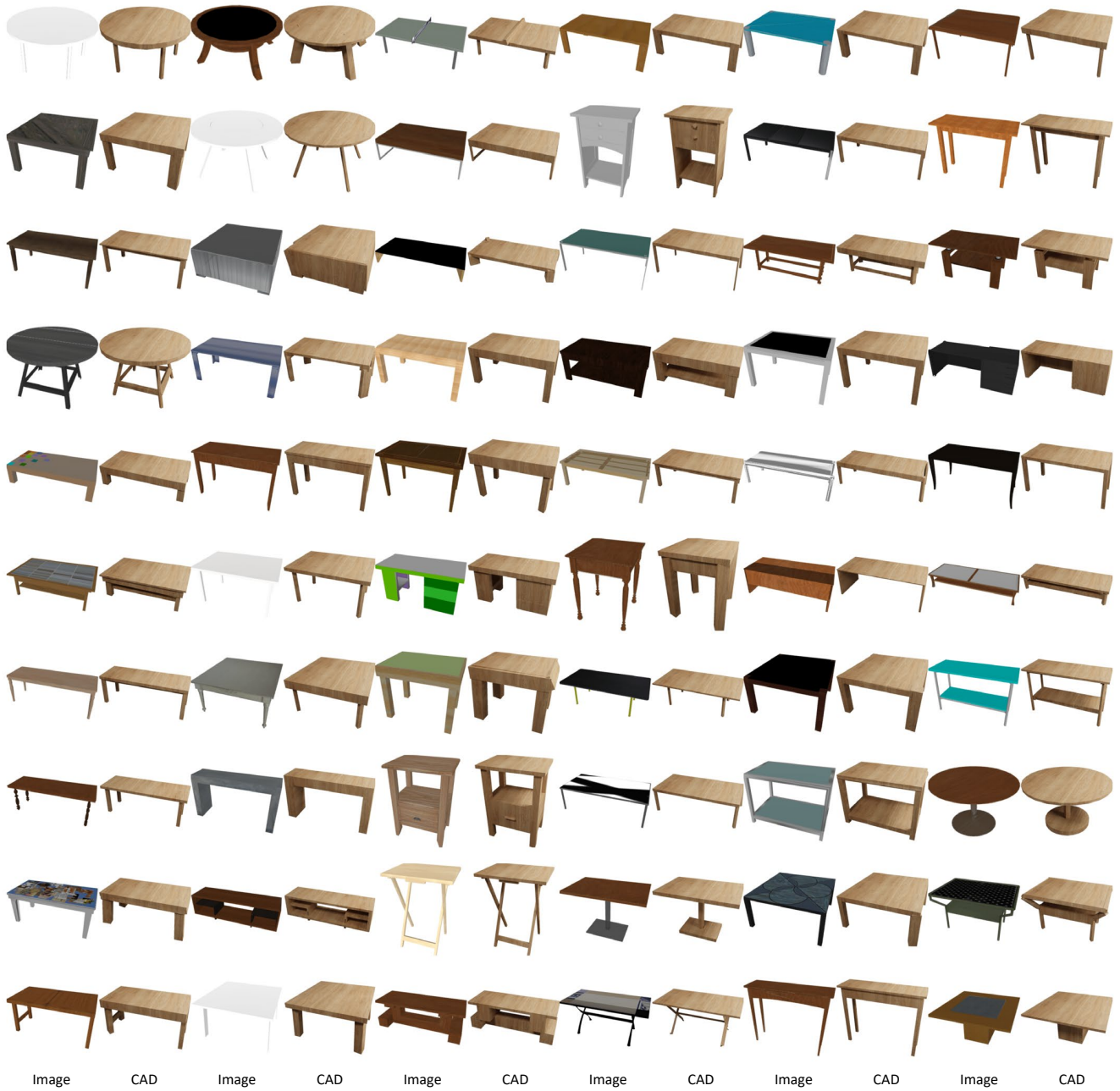


Figure A5: Dataset visualizations for tables. For each pair, left: ShapeNet model, right: our CAD-ified model.



Figure A6: Dataset visualizations for cabinets. For each pair, left: ShapeNet model, right: our CAD-ified model.

A.5 Limitations and Future Work

While CAD models are often used for mechanical parts, we found that VLMs perform less effectively on images of such objects. We intend to address this issue using in-context learning and LLM/VLM fine-tuning in future work. Additionally, GPT-4V sometimes makes mistakes and fails to provide the exact number of parts seen in the image, as shown in Figure A7.



Figure A7: Failure cases. GPT-4V can sometimes hallucinate or miss some structural parts. For each pair, left: input image; right: our model prediction.